

Coupling photocatalytic water oxidation with reductive transformations of organic molecules

Received: 4 September 2021

Accepted: 3 October 2022

Published online: 19 October 2022

Check for updates

Xinzhe Tian^{1,2}, Yinggang Guo^{1,2}, Wankai An¹, Yun-Lai Ren¹✉, Yuchen Qin¹, Caoyuan Niu¹ & Xin Zheng¹

The utilization of readily available and non-toxic water by photocatalytic water splitting is highly attractive in green chemistry. Herein we report that light-induced oxidative half-reaction of water splitting is effectively coupled with reduction of organic compounds, which provides a light-induced avenue to use water as an electron donor to enable reductive transformations of organic substances. The present strategy allows various aryl bromides to undergo smoothly the reductive coupling with Pd/g-C₃N₄* as the photocatalyst, giving a pollutive reductant-free method for synthesizing biaryl skeletons. Moreover, the use of green visible-light energy endows this process with more advantages including mild conditions and good functional group tolerance. Although this method has some disadvantages such as a use of environmentally unfriendly 1,2-dioxane, an addition of Na₂CO₃ and so on, it can guide chemists to use water as a reducing agent to develop clean procedures for various organic reactions.

Reductive couplings of aryl halides are of great significance in modern organic synthesis because the resulting biaryl skeletons are widely found in dyes, natural products, pharmaceutical compounds, and optoelectronic molecules^{1,2}. As a result, considerable efforts have been devoted to the development of various methods for the reductive couplings^{2,3}, where alcohols, amines, formate salt, hydrazine hydrate, magnesium, and solvents were permitted to serve as the reductants^{1–8}. Recently, the photocatalytic strategies become popular due to their advantages, including mild reaction conditions and the use of green solar energy. For example, chemists have used photoredox or semiconductor catalysts to enable homo-couplings of aryl halides in the presence of reductants, e.g. triethylamine, *N,N*-diisopropylethylamine and methanol^{2,3,9–11}.

Compared with the above-mentioned reducing agents, water is more attractive in green chemistry due to its readily available, non-toxic, and non-flammable features^{12,13}. Thus, much attention has been devoted to applications of water in various fields, e.g. organic reactions with water as the solvent^{14–19}, hydrogen production by water splitting, and so on^{20–28}. Recently, several uses of water in organic synthesis have

been developed via the challenging photocatalytic water splitting. As shown in Fig. 1a, the first kind is the utilization of water as the oxygen source for the oxygenation of organic molecules by coupling the oxygenation with light-induced water oxidation half-reaction where oxidants such as [Co^{III}(NH₃)₅Cl]²⁺ and (NH₄)₂Ce(NO₃)₆ have been added as the electron acceptor^{29–32}. Subsequently, additional oxidant-free methods have been developed for the oxygenation of olefin and benzene C–H bonds by coupling the oxygenation with the two half-reactions of the water splitting (Fig. 1a)^{31,32}. The second kind is the proton reduction half-reaction coupled with oxidation of organic compounds (Fig. 1b)^{33–36}, and has provided a strategy for oxidative transformations of alcohols, thiols, and benzylamines^{33–36}. The third kind is that the proton reduction is coupled with the hydrogenation (Fig. 1c)^{37–40}, showing the use of water as the hydrogen source for the hydrogenation of olefins, nitro compounds, aldehydes, and halogenated compounds, in which reductants such as metal powders, triethanolamine, Na₂SO₃ and so on have been added to reduce H₂O to hydrogen. Similar methods have also been applied in the deuteration of halogenated compounds with D₂O^{39,40}. To our knowledge, there is

¹College of Science, Henan Agricultural University, Zhengzhou, Henan 450002, P.R. China. ²These authors contributed equally: Xinzhe Tian, Yinggang Guo.

✉ e-mail: renyunlai@126.com

no report regarding coupling photocatalytic water oxidation half-reaction with the reduction of organic compounds (Fig. 1d) before submitting this manuscript. Therefore, we focused on overcoming this challenge to develop a method for using water as the reductant to enable the reductive coupling of aryl bromides.

On the other hand, graphite phase carbon nitride (g-C₃N₄)-based materials have been emerging as attractive photocatalysts for the hydrogen evolution^{33–36,41,42}, the water oxidation^{43,44}, oxidative degradation of pollutants, and the CO₂ reduction^{45,46}, due to the unique electronic band structure, high thermal and chemical stability of g-C₃N₄. In addition, this kind of materials has frequently served as photocatalysts for organic reactions, including reductive^{27,47}, oxidative, and nonredox reactions of organic molecules^{48–51}, encouraging us to select transition metal/g-C₃N₄ to make our idea come true.

In this work, we report that light-induced oxidative half-reaction of water splitting is effectively integrated with the reductive coupling of aryl bromides in the presence of the activated Pd/g-C₃N₄ (named as Pd/g-C₃N₄^{*}) and Na₂CO₃, which provides a method for using green water as the reductant to enable the reductive coupling. Moreover, the use of visible-light as green energy endows this process with more advantages, including mild conditions, good functional group tolerance, and broad substrate applicability.

Results

Preparation and characterization of photocatalysts

Pd/g-C₃N₄ was prepared based on previous literatures^{38,40}. In order to improve the catalytic activity, Pd/g-C₃N₄ was irradiated by blue light in the presence of Na₂CO₃ and H₂O to give Pd/g-C₃N₄^{*}. According to the TEM image (Supplementary Figs. 1 and 2), the Pd nanoparticles in Pd/g-C₃N₄^{*} are uniformly dispersed and has a narrow size distribution in the range of 5–10 nm. In addition, there is a slight difference between the

Pd nanoparticles size of Pd/g-C₃N₄^{*} and that of Pd/g-C₃N₄ (Supplementary Fig. 2), suggesting that the light-irradiated treatment had a slight effect on the distribution of the Pd nanoparticles. As seen from X-ray diffraction patterns (Supplementary Fig. 3), the diffraction peaks from Pd had little change when Pd/g-C₃N₄ was activated by our method, which reveals that the activating treatment would not result in significant leaching losses of Pd nanoparticles.

Next, the light capture capacity of the two catalysts was precisely examined by UV-visible diffuse reflection spectra. As shown in Fig. 2a, Pd/g-C₃N₄^{*} displays a broader photoresponse performance that ranges from 200 to 750 nm, and the maximum absorption is centered at 200–380 nm. Compared with Pd/g-C₃N₄, Pd/g-C₃N₄^{*} exhibits a slightly increase in adsorption at 450–750 nm wavelengths. The results from the calculation via the Tauc function show that the optical band gaps of Pd/g-C₃N₄ and Pd/g-C₃N₄^{*} are 2.51 eV and 2.53 eV, respectively (Supplementary Fig. 4b). The conduction band (CB) positions vs. normal hydrogen electrode (NHE) were also clarified via electrochemical Mott-Schottky experiments (Supplementary Fig. 5), and the results show that the CB in two cases are –0.90 V and –0.81 V (Fig. 2b), respectively, ignoring the difference between the flat band gap and the CB. Thus the valence band (VB) positions in two cases can be estimated to be 1.61 V and 1.72 V, respectively (Fig. 2b), revealing that the electronic band structure of the catalyst had a slight change after our activating treatment.

We examined the chemical state of Pd by X-ray photoelectron spectroscopy (XPS). As shown in Supplementary Fig. 6, the deconvoluted peaks related to the 3d_{3/2} and 3d_{5/2} orbitals of Pd⁰ are 340.23 and 335.00 eV⁵², while another two shoulder peaks should be assigned to Pd^{II} in PdO⁵². Based on the area of the peaks, the percentages of Pd⁰ in the Pd nanoparticles are 54% for Pd/g-C₃N₄ and 73% for Pd/g-C₃N₄^{*}, respectively (Supplementary Fig. 6), which indicates that our activating treatment can increase the percentage of Pd⁰. We examined the evolved gas and the results show that the molar ratio of the evolved O₂, H₂ and the increasing Pd⁰ is 0.5:0.3:0.7, which reveals that about 70% of electrons from the OER half-reaction (2OH[–] → 0.5O₂ + H₂O + 2e[–]) enable the formation of Pd⁰ (Pd^{II} + 2e[–] → Pd⁰), suggesting the OER half-reaction serves as the sacrificial electron donor for conversion of Pd^{II} to Pd⁰. Thus a rough mechanism for the Pd⁰ formation is presented in Fig. 2c based on the OER mechanism (see below) and the observation above.

Effect of various conditions on the reductive coupling

As shown in Fig. 3a, the reductive coupling didn't occur in the case of bare g-C₃N₄, while the deposition of 2.8 wt% Pd on g-C₃N₄ gave the biphenyl product in 4% yield, suggesting that the Pd species served as the catalytic sites. Other transition metals, including Pt, Ni, and Cu supported on g-C₃N₄ were also test, but no targeted product was observed. Subsequently, we found that the yield increased

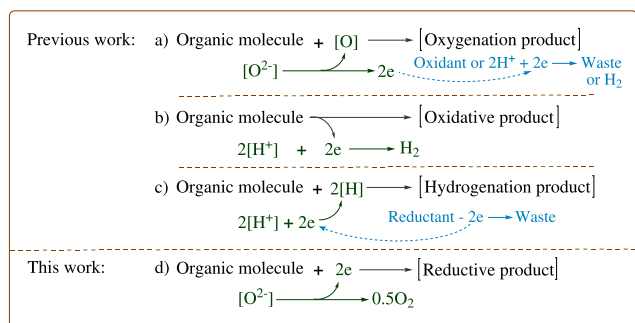


Fig. 1 | Background of this work. Organic reactions with H₂O as the oxygen source (a), the oxidant (b), the hydrogen source (c) or the electron donor (d).

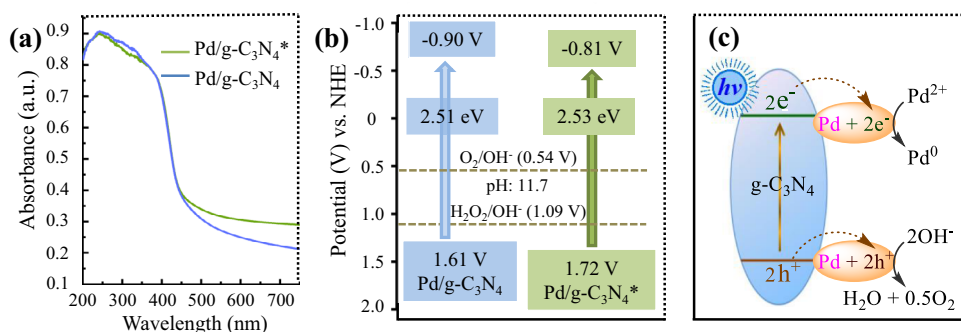


Fig. 2 | Effect of the light-irradiated treatment on Pd/g-C₃N₄. a UV-visible diffuse reflection spectra of Pd/g-C₃N₄ (blue curve, 2.8 wt%) and Pd/g-C₃N₄^{*} (green curve, 2.8 wt%). a.u.: arbitrary units. Source data are provided as a Source Data file.

b Energy-band positions of Pd/g-C₃N₄ (blue, 2.8 wt%) and Pd/g-C₃N₄^{*} (green, 2.8 wt%). **c** Rationale for conversion of Pd^{II} to Pd⁰. Pd/g-C₃N₄^{*}: the activated Pd/g-C₃N₄ by the light-irradiated treatment.

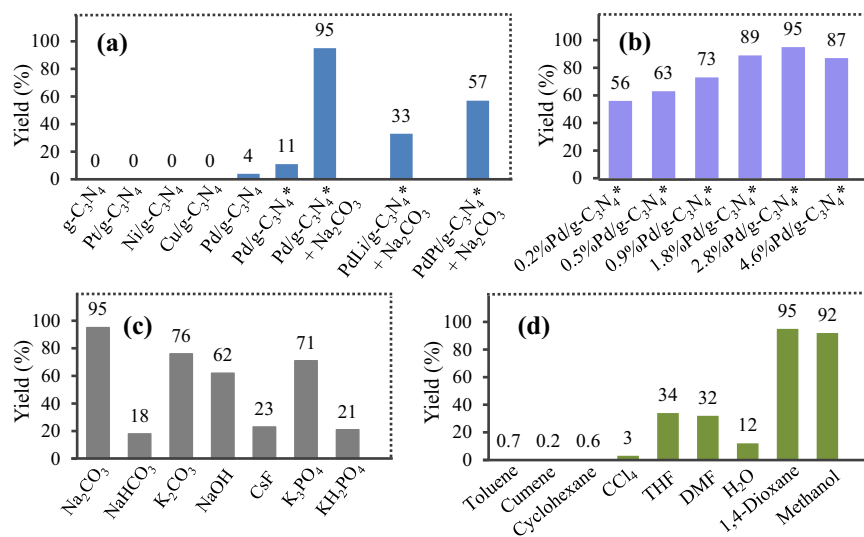


Fig. 3 | Effect of different conditions on the coupling of bromobenzene. a Effect of different photocatalyst systems. The loading of the metal on g-C₃N₄ is 2.8 wt% in all cases. M/g-C₃N₄: graphite phase carbon nitride-supported metal, M/g-C₃N₄*: the activated Pd/g-C₃N₄ by the light-irradiated treatment. **b** Effect of different Pd loading amounts. x%/g-C₃N₄* means that the loading of Pd on g-C₃N₄ is x wt%.

c Effect of different bases. Yield: yield of biphenyl. **d** Effect of different solvents. THF: tetrahydrofuran, DMF: *N,N*-dimethylformamide. For experimental procedures and conditions, see Unit 1.4.2, 1.4.3, and 1.4.4 in the supplementary information. Source data are provided as a Source Data file.

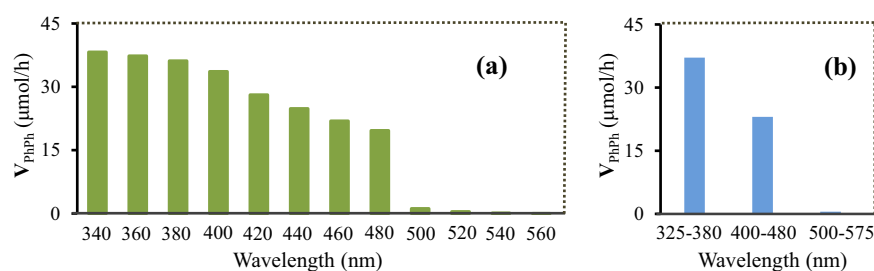


Fig. 4 | Coupling of bromobenzene under different wavelengths of light. a Effect of different monochromatic lights on the produced rate of biphenyl. x nm wavelength represents x ± 10 nm wavelength. **b** Effect of different polychromatic lights

on the produced rate of biphenyl. V_{PhPh} represents the produced rate of biphenyl. For experimental procedures and conditions, see Unit 1.4.5 in the supplementary information. Source data are provided as a Source Data file.

significantly when Pd/g-C₃N₄ was irradiated with blue light prior to the addition of substrate, which indicates that the irradiating process can slightly enhance the catalytic ability of Pd/g-C₃N₄. To our delight, an addition of Na₂CO₃ resulted in a remarkable increase in the biphenyl yield. PdLi/g-C₃N₄* and PdPt/g-C₃N₄* were also examined as the catalysts, but the targeted product was obtained in only 33% and 57% yields, respectively. Subsequently, effect of the Pd loading on the reaction was investigated, and the results in Fig. 3b show that 2.8 wt% Pd loading is optimum. The yield significantly increased with increasing the Pd loading to 2.8 wt%. However, when the Pd loading increased from 2.8 to 4.6 wt%, the yield dropped, which is possibly rationalized by assuming that aggregation of excess Pd nanoparticles would lead to charge recombination³⁸.

Among the screened bases, Na₂CO₃ was the most effective (Fig. 3c). Low yields were obtained in the case of using more weakly alkaline, including NaHCO₃ and KH₂PO₄, while Na₂CO₃, K₂CO₃, K₃PO₄, and NaOH allowed the reaction to proceed with 62–95% yields, which indicates that the basicity has an important effect on the reaction. The reaction was highly dependent on the solvent type (Fig. 3d). The solvents, including toluene, cumene, cyclohexane, and CCl₄ were less effective, possibly due to the poor dispersion of the catalyst in these solvents. On the contrary, the catalyst could be effectively dispersed in 1,4-dioxane and methanol, which allowed the coupling to proceed smoothly.

Effect of the wavelength variation on the reaction was also investigated. As seen from Fig. 4a and Supplementary Figs. 9–11, both the rate of the biphenyl production and the apparent quantum efficiencies decreased with increasing the wavelength in the range from 340 ± 10 nm to 480 ± 10 nm, which is consistent with the variation tendency regarding the photoabsorption of the catalyst (Fig. 2a), revealing that the reaction rate is dependent on the photoresponse of the catalyst, and that the present coupling reaction is mainly triggered by the photoexcitation of the catalyst. As shown in Figs. 4a and 2a, when the wavelength exceeded the photoabsorption edge (490 nm) of Pd/g-C₃N₄* semiconductor, the coupling reaction was very sluggish in spite of an evident photoresponse of the catalyst (for the reasons behind these results, see Supplementary Note 1), which coincides with the assumption that the coupling reaction is mainly driven by the light-induced separation of electron-hole pairs in the semiconductor (for the detailed explanations, see Supplementary Note 1). Afterwards, we performed the reaction under irradiation of the light having a broad illumination spectrum. As seen from Fig. 4b, 325–380 nm polychromatic UV light allowed biphenyl to be produced in higher rate than that in the case of 400–480 nm polychromatic blue light, which is attributed to that the catalyst exhibits a stronger response to 325–380 nm UV light than to the blue light (Fig. 2a). The substrate was less reactive in the case of using more than 490 nm polychromatic light, which is consistent with the above performance of the monochromatic light.

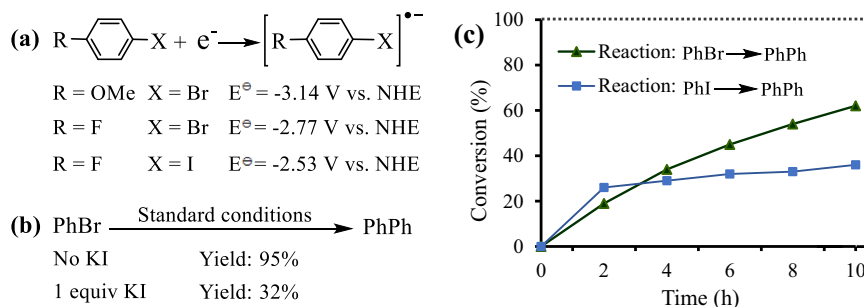


Fig. 6 | Effect of substituents or halogen ions. **a** Standard redox potential (E) of phenyl halides with different substituents. NHE represents a normal hydrogen electrode. **b** Effect of I⁻ on the reaction. For standard conditions, see Fig. 5. **c** Time

course of the conversion of bromobenzene (green) and iodobenzene (blue). PhBr: bromobenzene, PhI: iodobenzene, PhPh represents biphenyl. Source data are provided as a Source Data file.

(a) $2\text{PhBr} \xrightarrow{\text{Standard conditions}}$ PhPh

Condition	Conv.	Yield
No H ₂ O	5%	Trace
No Pd/g-C ₃ N ₄ *	< 1%	No
No 1,4-dioxane	18%	15%
No light, 40 or 100 °C	1-6%	No

(b) $2\text{PhBr} \xrightarrow[2\text{ h, } h\nu]{\text{Standard conditions}}$ PhPh

Temperature	Conv.	\bar{V}_{PhPh}
0 °C	16%	18 μmol/h
25 °C (RT)	21%	25 μmol/h
50 °C	27%	32 μmol/h
80 °C	39%	46 μmol/h

Fig. 7 | Several control experiments. **a** Investigation on the necessity for using water, Pd/g-C₃N₄*, 1,4-dioxane, and light. PhBr: bromobenzene, PhPh: biphenyl, Conv.: conversion of bromobenzene, Yield: yield of biphenyl. **b** Effect of temperature on the reaction. \bar{V}_{PhPh} : the average rate of biphenyl production in 2 h. For standard conditions, see Fig. 5.

bromides under irradiation of UV-light (350 ± 10 nm light or 325–380 nm polychromatic light) and blue light (400–480 nm polychromatic light). Compared with the blue light, the UV-light allowed all the substrates to be completely converted in shorter time (Supplementary Table 3), due to that the catalyst exhibits a stronger response to UV-light than to the blue light (Fig. 2a). It is worth noting that the aldehyde substituent is easily destroyed under irradiation of UV-light (see 2c in Supplementary Table 3), owing to that the energy of UV-light photons is enough high to enable the homolysis of C-H bond in the aldehyde group in the absence of photocatalysts⁵⁴.

As shown in Supplementary Tables 4 and 5, the most noteworthy characteristic of the present method is the use of green water as the reductant in the reductive couplings (entry 1 vs. entries 2–19)^{1,5–9,55–60}. Moreover, the use of visible-light in our method endows this process with more advantages, including mild conditions and green energy (Supplementary Table 4, entry 1). Compared with other reductive aryl-aryl couplings (Supplementary Table 5, entries 2–19)^{1,5–9,55–60}, the present reaction exhibited better functional group tolerance (Supplementary Table 5, entry 1). In addition, our method showed broader substrate applicability and allowed various phenyl, naphthyl, thienyl, and pyridinyl bromides to undergo the reductive coupling smoothly, whereas only phenyl and naphthyl bromides were tested in some of literatures^{5–7,9,59,60}. Unfortunately, our method couldn't be applied in the biaryl cross-coupling between different aryl halides, and inert aryl chlorides were less reactive under our conditions.

Investigation on the recycling of Pd/g-C₃N₄*, the reproducibility of the catalyst and the necessity for using Pd/g-C₃N₄*, water, 1,4-dioxane, light, and heat

As shown in Supplementary Fig. 14, the catalyst could be recycled for three times with a very slight change in the catalytic activity (for the main reasons why the catalytic efficiency would decrease after four cycling runs, see Supplementary Note 2). When eight different batches of the catalyst were respectively used, the targeted product was obtained in high yields ranging from 92% to 96% (Supplementary

Table 6), suggesting that the results regarding the catalytic activity of Pd/g-C₃N₄* are reliable and reproducible. The results from six parallel experiments regarding the coupling of bromobenzene also reveal that the reported results in the present paper are reliable and reproducible (Supplementary Table 7). As shown in Fig. 7a, hardly any coupling product was observed in the absence of water or Pd/g-C₃N₄*, indicating that both water and Pd/g-C₃N₄* were indispensable for the reaction. The absence of 1,4-dioxane would lead to poor dispersion of the catalyst in the solvent, thus the reaction didn't go well in the pure water (Fig. 7a), which reveals that 1,4-dioxane served as the dispersant in the present reaction. We also performed the control experiments without irradiation, and the results show that the coupling wouldn't occur under irradiation-free conditions (Fig. 7a), suggesting that the irradiation of light is indispensable for the present reaction. This conclusion was also supported by the following results: the coupling rate linearly increased with increasing the light intensity (Supplementary Fig. 20). This approximately linear relationship is often reported in literatures regarding g-C₃N₄ semiconductor-catalyzed organic reactions⁶¹, and indicates that the reaction is dominated by a single photon absorption event⁶¹. Similar to many photocatalytic reactions^{45,46}, the coupling rate would increase with raising the reaction temperature (Fig. 7b).

Investigation on who serves as the electron-donor in the reductive coupling

We inferred that water served as the electron donor by the oxidation of H₂O to O₂ under our conditions. Indeed, the formation of ¹⁸O₂ was observed in the H₂¹⁸O-labelling experiment where H₂¹⁸O was added into the reaction system (Supplementary Fig. 21a). Maybe the resulting Br⁻ played the role of the electron donor via conversion of Br⁻ to Br₂, but this possibility was ruled out based on our experimental results: No Br₂ was detected after reaction (Supplementary Fig. 21c). In addition, it is possible that dioxane or the benzene ring served as the electron donor by the oxidation of them (Supplementary Fig. 21d). To rule out this possibility, we analysed the reaction system using GC-MS and HPLC-MS, but no detectable amount of products from the oxidation of dioxane or the benzene ring was observed. Obviously, the experimental results above confirm the reliability of our conclusion that only water serves as the electron donor in our reactions.

Reason why the light illumination of Pd/g-C₃N₄ slightly improves the catalytic activity

As stated above, we irradiated Pd/g-C₃N₄ with blue light prior to the addition of aryl halides. Such a treatment would result in a conspicuous increase in the ratio of Pd⁰ to Pd^{II} (Supplementary Fig. 6), but didn't lead to remarkable changes in the distribution of the Pd nanoparticles, the light capture capacity and the electronic band structure (see Fig. 2). In addition, when different batches of the catalyst were

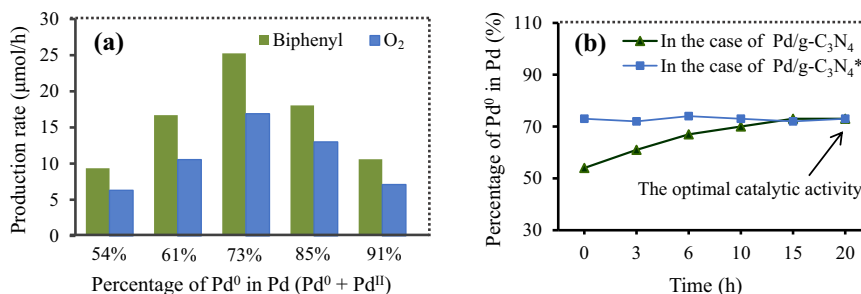


Fig. 8 | Relationship between the Pd⁰ concentration and the coupling. **a** Effect of the percentage of Pd⁰ on the average rate of the biphenyl (green) and O₂ (blue) production in 2 h. **b** Time course of the Pd⁰ concentration in the case of Pd/g-C₃N₄

(green) or Pd/g-C₃N₄* (blue). For experimental procedures, see Unit 1.6 and 1.7 in the supplementary information. Source data are provided as a Source Data file.

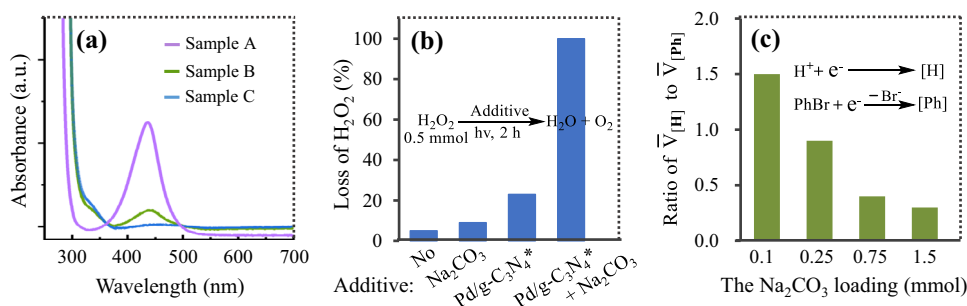


Fig. 9 | Investigation on the role of Na₂CO₃. **a** UV-Vis spectroscopy related to the produced H₂O₂ in the coupling of bromobenzene. Sample A (purple curve): 0.4 mmol/L aqueous solution of H₂O₂, Sample B (green curve): the produced H₂O₂ under standard conditions (no Na₂CO₃) in Fig. 5, Sample C (blue curve): the produced H₂O₂ under standard conditions in Fig. 5, a.u.: arbitrary units. **b** The H₂O₂

decomposition in the presence of additives. **c** Effect of the Na₂CO₃ loading on the ratio of $\bar{V}_{[H]}$ to $\bar{V}_{[Ph]}$. PhBr: bromobenzene. [Ph]: intermediate regarding phenyl radical, [H]: intermediate regarding hydrogen radical. $\bar{V}_{[H]}$ and $\bar{V}_{[Ph]}$ represents the average rate of the [H] and [Ph] production in 4 h, respectively. Source data are provided as a Source Data file.

used, the yields of the coupling product fluctuated in a narrow range (Supplementary Table 6), suggesting that small changes in the distribution of the Pd nanoparticles wouldn't be highly influential of the catalytic activity (Supplementary Note 3). These evidences reveal that the increase in the Pd⁰ concentration is the main reason why the catalytic activity is slightly improved. In theory, an increase in the percentage of Pd⁰ should be advantageous to the coupling half-reaction because Pd⁰ is the indispensable species for catalyzing this half-reaction^{62,63}. However, with increasing the percentage of Pd⁰, the percentage of Pd^{II} would decrease, which should be disadvantageous to the water oxidation half-reaction because Pd^{II} serves as the catalytically active species for this half-reaction⁶⁴. Thus both too-low and too-high percentages of Pd⁰ should be unfavorable to the overall reductive coupling reaction. Indeed, the production rate of biphenyl increases with increasing the percentage of Pd⁰ in Pd (Pd⁰ + Pd^{II}) to the optimum value (73%) and then decreases (see Fig. 8a). We monitored the change of the Pd⁰ concentration throughout the reductive coupling (Fig. 8b), and the results reveal that the percentage of Pd⁰ in the case of Pd/g-C₃N₄ is still less than the optimum value (73%) regarding the catalytic activity in 10 h. It is also worth noting that increasing the Pd⁰ concentration would suppress the formation of benzene byproduct (Supplementary Table 8). Based on these observations, it can be concluded that the illuminating treatment of Pd/g-C₃N₄ prior to the addition of aryl halides makes the Pd⁰ concentration reach the optimum value in a short time (2-3 min), which not only slightly improves its catalytic activity, but also suppresses the formation of the benzene byproduct.

Reason why Na₂CO₃ has a positive effect on the present reaction

According to previous literatures^{65,66}, the water oxidation often yields H₂O₂, and Na₂CO₃ can regenerate the photocatalysts by removing the

resulting H₂O₂ that poisons metal/g-C₃N₄^{65,66}. To verify this possibility, we analysed the reaction system using UV-Vis spectroscopy with *o*-tolidine as the indicator of H₂O₂. It is worth noting that the peak at 438 nm is a typical absorption peak that confirms H₂O₂⁶⁶. As shown in Fig. 9a, H₂O₂ was observed for Na₂CO₃-free reaction system after Pd/g-C₃N₄*-catalyzed coupling was performed, while H₂O₂ disappeared in the reaction system in the presence of Na₂CO₃. These results suggest that the positive effect of Na₂CO₃ on the reaction is due to that it can remove the produced H₂O₂, or suppress the formation of H₂O₂ that poisons our photocatalyst. This conclusion is also verified by the evidences related to the formation mechanism of H₂O₂ in literatures^{65,66}, and the following results (Fig. 9b): Both Na₂CO₃ and Pd/g-C₃N₄* were less effective to catalyze the H₂O₂ decomposition, whereas the simultaneous presence of Pd/g-C₃N₄* and Na₂CO₃ resulted in a complete decomposition of H₂O₂. As shown in Fig. 9c, the ratio of $\bar{V}_{[H]}$ to $\bar{V}_{[Ph]}$ becomes smaller and smaller with increasing the Na₂CO₃ concentration, suggesting that Na₂CO₃ can suppress the H⁺ reduction, which possibly attributes to that an addition of Na₂CO₃ decreases the H⁺ concentration in the reaction system. Thus it can be concluded that an inhibition effect of Na₂CO₃ on the undesired H⁺ reduction is also one of the main reasons why Na₂CO₃ can promote the reaction.

Reaction mechanism for the reductive coupling

Two kinds of mechanisms for the reductive coupling have been proposed in the previous literatures. One undergoes the oxidative addition of aryl halides to the transition metals^{1,3,11}. The other starts with the formation of the aryl radical anion (ArX^{•-}) by the single electron transfer (SeT) from catalysts to aryl halides^{3,39,40,67}. Considering that most of light-induced reductive couplings undergo the SeT mechanism pathways^{3,39,40,67}, we guessed that the present reaction involved some radical-like species. Indeed, the presence of the

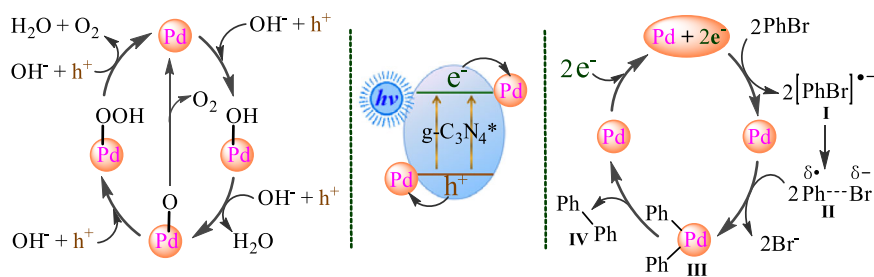


Fig. 10 | Proposed mechanism. Photocatalytic reductive coupling of bromobenzene using Pd/g-C₃N₄*. PhBr: bromobenzene, h⁺: hole, e⁻: electron.

radical inhibitor 2,2,6,6-tetramethyl-1-piperidinyloxy or 2,6-ditbutyl-4-methylphenol would prevent the targeted product from being produced (Supplementary Fig. 27a). According to previous literatures^{1,2}, the oxidative addition of aryl halides to the Pd⁰ species can occur under thermal conditions, hence light-free conditions should allow the reductive coupling to proceed smoothly in the presence of stoichiometric Pd⁰ species as the electron-donor. On the contrary, when 1 equiv Pd⁰ species contained in the catalyst was used, the light-free coupling of bromobenzene didn't occur at 100 °C (Supplementary Fig. 27b), suggesting that the oxidative metal addition-based mechanism should be ruled out.

Based on the observations above, a radical mechanism pathway is proposed with the coupling of bromobenzene as the representative. As shown in Fig. 10, g-C₃N₄ acts as the light absorber^{41,42}, and its electrons are excited from the valence band (VB) to the conduction band (CB) upon irradiation with light. On the one hand, electrons of the CB of g-C₃N₄ transfer to Pd⁰ atoms that are just the active sites for the reductive coupling, which has been confirmed in many literatures^{62,63}. Then intermediate I is produced via the electron transfer under assistance of Pd nanoparticles^{1,2,11}, followed by the production of phenyl radical-like species II^{1,2,11}. Next, the reaction between Pd and two molecules of species II provides diphenylpalladium III^{1,2,11}. Finally, intermediate III undergoes reductive elimination to provide the targeted product^{1,2,11}.

Subsequently, our attention was paid to clarifying the mechanism of the oxygen evolution (OER) half-reaction. Two kinds of pathways for the water oxidation to O₂ have been proposed in the previous literatures^{65,66}. One is the four-electron one-step process (Supplementary Fig. 28a)⁶⁸, and the other proceeds via 2e⁻/2e⁻ two-step process (Supplementary Fig. 28b)^{65,66}. According to the bandgap structure of Pd/g-C₃N₄* (see Fig. 2b), both the two processes are thermodynamically permitted. Thus we performed the rotating ring-disk electrode experiments to confirm the mechanism pathway. The electron-transfer number is 4 for the one-step process and 2 for the two-step process⁶⁵, while our results show that the electron-transfer numbers range from 3.49 to 3.54 which are close to 4 (Supplementary Fig. 29), suggesting that the one-step process serves as the major pathway under our conditions. Thus a mechanism (see Fig. 10) is proposed based on the above observations and conventional mechanisms of electrochemical OER under alkaline conditions⁶⁸.

Discussion

In this work, we report that water is used as the electron-donor to enable the reductive transformations of organic molecules by coupling the light-induced water oxidation half-reaction with the reduction of organic compounds in the presence of Pd/g-C₃N₄* photocatalyst. The used photocatalyst is in-situ synthesized by a method where Pd/g-C₃N₄ is irradiated by the light in the presence of Na₂CO₃ and H₂O. Such a treatment can slightly improve the activity of Pd/g-C₃N₄ by increasing the ratio of Pd⁰ to Pd^{II}. In addition, our experimental results reveal that Na₂CO₃ has a considerably positive effect on the reaction by inhibiting the proton reduction and removing

the produced H₂O₂ that poisons our photocatalyst. The present strategy allows various aryl bromides to undergo smoothly the reductive coupling under catalysis of Pd/g-C₃N₄*, providing a pollutive reductant-free method for synthesizing biaryl skeletons. Moreover, the use of visible-light as the green energy endows this process with more advantages including mild conditions, good functional group tolerance, and broad substrate applicability. Unfortunately, the present method has some disadvantages, such as the use of environmentally unfriendly 1,2-dioxane and an addition of Na₂CO₃. However, we believe that these results can guide chemists to use water as a reductant to develop clean procedures for various organic reactions by changing the composition of the semiconductor photocatalyst.

Methods

Procedure for preparation of Pd/g-C₃N₄

After 50 mg g-C₃N₄ were added to a 100 mL flask equipped with 50 mL ethanol, the system was sonicated for 3 h to make g-C₃N₄ to be dispersed in ethanol. Then 100 mL K₂PdCl₆ solution (0.01 M) was added, and the mixture was stirred for 10 min. Subsequently, 5 mL of water was added, and the mixture was refluxed at 90 °C for 1 h. Finally, the reaction mixture was cooled to room temperature, the precipitation was collected, washed with ethanol, dried at 60 °C under reduced pressure to give Pd/g-C₃N₄.

Procedure for preparation of Pd/g-C₃N₄*

15.00 mg Pd/g-C₃N₄ and 79.50 mg Na₂CO₃ were added to a 10 mL quartz glass tube equipped with 5 mL H₂O, 3 mL 1,4-dioxane, and a magnetic stirring under argon atmosphere. Then the reaction mixture was magnetically stirred for 2–3 min under the irradiation (light source: 420 ± 10 nm LED, incident light intensity: 0.15 W/cm²). Once the reaction time was reached, the precipitate was filtrated and washed in turn with water and ethanol. The collected solid was dried at 80 °C under reduced pressure to give Pd/g-C₃N₄*.

General procedure for the reductive coupling

15.0 mg Pd/g-C₃N₄ and 79.5 mg Na₂CO₃ were added to a 10 mL quartz glass tube equipped with 5 mL H₂O and 3 mL 1,4-dioxane under argon atmosphere. After the reaction mixture was magnetically stirred for 2–3 min under the irradiation (light source: 420 ± 10 nm LED, incident light intensity: 0.15 W/cm²). Note: according to our measurement results, when the power of the light source was set as 75 W, the actual incident light intensity in the reaction tube was 0.15 W/cm² to give in-situ Pd/g-C₃N₄*, 0.5 mmol aryl bromide was added. Then the reaction tube was sealed and placed in a constant-temperature bath (25 °C) to perform the reductive coupling for 20 h under the irradiation (light source: 420 ± 10 nm LED, incident light intensity: 0.15 W/cm²) and argon atmosphere. Once the reaction time was reached, GC analysis of the mixture provided GC yields. The crude product from another parallel experiment was purified by silica gel chromatography to give the desired product.

Characterization

The photocatalysts were characterized by transmission electron microscope (TEM), X-ray photoelectron spectroscopy (XPS), X-ray diffraction patterns, UV-Vis spectroscopy. The reductive coupling products were confirmed by $^1\text{H-NMR}$ and $^{13}\text{C-NMR}$ spectra. The details of these techniques and the other experimental procedure were shown in the supplementary information.

Data availability

The data that support the findings of this study are available within the paper and its supplementary information files. Extra data are available from the author upon request. Source data are provided with this paper.

References

- Gong, X. C. et al. Ligand-free palladium catalyzed Ullmann biaryl synthesis: "household" reagents and mild reaction conditions. *Green Chem.* **21**, 995–999 (2019).
- Jiang, J., Du, L. Y. & Ding, Y. Q. Aryl-aryl bond formation by Ullmann reaction: from mechanistic aspects to catalyst. *Mini-Rev. Org. Chem.* **17**, 26–46 (2020).
- Hassan, J., Sevignon, M., Gozzi, C., Schulz, E. & Lemaire, M. Aryl-aryl bond formation one century after the discovery of the Ullmann reaction. *Chem. Rev.* **102**, 1359–1470 (2002).
- Karimi, B., Barzegara, H. & Vali, H. Au–Pd bimetallic nanoparticles supported on a high nitrogen-rich ordered mesoporous carbon as an efficient catalyst for room temperature Ullmann coupling of aryl chlorides in aqueous media. *Chem. Commun.* **54**, 7155–7158 (2018).
- Zuo, Z., Kim, R. S. & Watson, D. A. Synthesis of axially chiral 2,2'-bisphosphobiarenes via a nickel-catalyzed asymmetric Ullmann coupling: general access to privileged chiral ligands without optical resolution. *J. Am. Chem. Soc.* **143**, 1328–1333 (2021).
- Rana, S., Varadwaj, G. B. B. & Jonnalagadda, S. B. Pd nanoparticle supported reduced graphene oxide and its excellent catalytic activity for the Ullmann C–C coupling reaction in a green solvent. *RSC Adv.* **9**, 13332–13335 (2019).
- Prasanna, Bhat, S. K., Usha, K. M. & Hegde, M. S. Ligand and base free synthesis of biaryls from aryl halides in aqueous media with recyclable $\text{Ti}_{0.97}\text{Pd}_{0.03}\text{O}_{1.97}$ catalyst. *Catal. Lett.* **151**, 3313–3322 (2021).
- Dhital, R. N. et al. Low-temperature carbon–chlorine bond activation by bimetallic gold/palladium alloy nanoclusters: an application to Ullmann coupling. *J. Am. Chem. Soc.* **134**, 20250–20253 (2012).
- Feizpour, F., Jafarpour, M. & Rezaeifard, A. Band gap modification of TiO_2 nanoparticles by ascorbic acid-stabilized Pd nanoparticles for photocatalytic Suzuki–Miyaura and Ullmann coupling reactions. *Catal. Lett.* **149**, 1595–1610 (2019).
- Lantern, A. E., Elhage, A. & Scaiano, J. C. Heterogeneous photocatalytic C–C coupling: mechanism of plasmon-mediated reductive dimerization of benzyl bromides by supported gold nanoparticles. *Catal. Sci. Technol.* **5**, 4336–4340 (2015).
- Crabbe, B. W., Kuehm, O. P., Bennett, J. C. & Hallett-Tapley, G. L. Light-activated Ullmann homocoupling of aryl halides catalyzed using gold nanoparticle-functionalized potassium niobium oxides. *Catal. Sci. Technol.* **8**, 4907–4915 (2018).
- Sun, F. et al. Energy-saving hydrogen production by chlorine-free hybrid seawater splitting coupling hydrazine degradation. *Nat. Commun.* **12**, 4182 (2021).
- Takata, T. et al. Photocatalytic water splitting with a quantum efficiency of almost unity. *Nature* **581**, 411–414 (2020).
- Meng, Q. L. et al. Sustainable production of benzene from lignin. *Nat. Commun.* **12**, 4534 (2021).
- Kitanosono, T., Xu, P. Y. & Kobayashi, S. Chiral Lewis acids integrated with single-walled carbon nanotubes for asymmetric catalysis in water. *Science* **362**, 311–315 (2018).
- Renders, T. et al. Catalytic lignocellulose biorefining in *n*-butanol/water: a one-pot approach toward phenolics, polyols, and cellulose. *Green Chem.* **20**, 4607–4619 (2018).
- Cortes-Clerget, M. et al. Water as the reaction medium in organic chemistry: from our worst enemy to our best friend. *Chem. Sci.* **12**, 4237–4266 (2021).
- Cortes-Clerget, M. et al. Bridging the gap between transition metal- and bio-catalysis via aqueous micellar catalysis. *Nat. Commun.* **10**, 2169 (2019).
- Cortes-Clerget, M., Lee, N. R. & Lipshutz, B. H. Synthetic chemistry in water: applications to peptide synthesis and nitro-group reductions. *Nat. Protoc.* **14**, 1108–1129 (2019).
- Service, R. F. New electrolyzer splits water on the cheap. *Science* **367**, 1181–1181 (2020).
- Ye, S. et al. Unassisted photoelectrochemical cell with multi-mediator modulation for solar water splitting exceeding 4% solar-to-hydrogen efficiency. *J. Am. Chem. Soc.* **143**, 12499–12508 (2021).
- Zhai, P. L. et al. Engineering single-atomic ruthenium catalytic sites on defective nickel-iron layered double hydroxide for overall water splitting. *Nat. Commun.* **12**, 4587 (2021).
- Yoon, K. Y. et al. NiFeO_x decorated Ge-hematite/perovskite for an efficient water splitting system. *Nat. Commun.* **12**, 4309 (2021).
- Wu, D. S. et al. Efficient overall water splitting in acid with anisotropic metal nanosheets. *Nat. Commun.* **12**, 1145 (2021).
- Sun, R. et al. Strain-engineered nano-ferroelectrics for high-efficiency piezocatalytic overall water splitting. *Angew. Chem. Int. Ed.* **60**, 16019–16026 (2021).
- Li, M. G. et al. Exclusive strain effect boosts overall water splitting in PdCu/Ir core/shell nanocrystals. *Angew. Chem. Int. Ed.* **60**, 8243–8250 (2021).
- Wen, F. et al. Amide-bridged conjugated organic polymers: efficient metal-free catalysts for visible-light driven CO_2 reduction with H_2O to CO. *Chem. Sci.* **12**, 11548–11553 (2021).
- Wu, Y. M. et al. Selective transfer semihydrogenation of alkynes with H_2O (D_2O) as the H (D) source over a Pd-P cathode. *Angew. Chem. Int. Ed.* **59**, 21170–21175 (2020).
- Hirai, Y. et al. Ruthenium-catalyzed selective and efficient oxygenation of hydrocarbons with water as an oxygen source. *Angew. Chem. Int. Ed.* **47**, 5772–5776 (2008).
- Fukuzumi, S., Kishi, T., Kotani, H., Lee, Y.-M. & Nam, W. Highly efficient photocatalytic oxygenation reactions using water as an oxygen source. *Nat. Chem.* **3**, 38–41 (2011).
- Singh, W. M. et al. Hydrogen production coupled to hydrocarbon oxygenation from photocatalytic water splitting. *Angew. Chem. Int. Ed.* **51**, 1653–1656 (2012).
- Zheng, Y.-W. et al. Photocatalytic hydrogen-evolution cross-couplings: benzene C–H amination and hydroxylation. *J. Am. Chem. Soc.* **138**, 10080–10083 (2016).
- Xie, S. J. et al. Visible light-driven C–H activation and C–C coupling of methanol into ethylene glycol. *Nat. Commun.* **9**, 1181 (2018).
- Wu, B. G. et al. Ultrathin porous carbon nitride bundles with an adjustable energy band structure toward simultaneous solar photocatalytic water splitting and selective phenylcarbinol oxidation. *Angew. Chem. Int. Ed.* **60**, 4815–4822 (2021).
- Li, X. B. et al. Mechanistic insights into the interface-directed transformation of thiols into disulfides and molecular hydrogen by visible-light irradiation of quantum dots. *Angew. Chem. Int. Ed.* **53**, 2085–2089 (2014).
- Liu, H., Xu, C. Y., Li, D. D. & Jiang, H.-L. Photocatalytic hydrogen production coupled with selective benzylamine oxidation over mof composites. *Angew. Chem. Int. Ed.* **57**, 5379–5383 (2018).
- Fan, X., Yao, Y. L., Xu, Y. S., Yu, L. & Qiu, C. T. Visible-light-driven photocatalytic hydrogenation of olefins using water as the H source. *ChemCatChem* **11**, 2596–2599 (2019).

38. Han, C. H. et al. Beyond hydrogen evolution: solar driven water-donating transfer hydrogenation over platinum/carbon nitride. *ACS Catal.* **10**, 9227–9235 (2020).
39. Liu, C. B. et al. Controllable deuteration of halogenated compounds by photocatalytic D₂O splitting. *Nat. Commun.* **9**, 80 (2018).
40. Ling, X. et al. A visible-light-photocatalytic water-splitting strategy for sustainable hydrogenation/deuteration of aryl chlorides. *Sci. China Chem.* **63**, 386–392 (2020).
41. Zhang, D. L. et al. Polymeric carbon nitride-derived photocatalysts for water splitting and nitrogen fixation. *Small* **17**, 2005149 (2021).
42. Kranz, C. & Wachtler, M. Characterizing photocatalysts for water splitting: from atoms to bulk and from slow to ultrafast processes. *Chem. Soc. Rev.* **50**, 1407–1437 (2021).
43. Wu, Q. Y. et al. A metal-free photocatalyst for highly efficient hydrogen peroxide photoproduction in real seawater. *Nat. Commun.* **12**, 483 (2021).
44. Zhao, Y. B. et al. Mechanistic analysis of multiple processes controlling solar-driven H₂O₂ synthesis using engineered polymeric carbon nitride. *Nat. Commun.* **12**, 3701 (2021).
45. Xie, K. L., Fang, J. F., Li, L., Deng, J. P. & Chen, F. F. Progress of graphite carbon nitride with different dimensions in the photocatalytic degradation of dyes: a review. *J. Alloy. Compd.* **901**, 163589 (2022).
46. Lu, Q. Q. et al. Engineering graphitic carbon nitride (g-C₃N₄) for catalytic reduction of CO₂ to fuels and chemicals: strategy and mechanism. *Green. Chem.* **23**, 5394–5428 (2021).
47. Pei, L. J. et al. Hydroxyl-group-modified polymeric carbon nitride with the highly selective hydrogenation of nitrobenzene to *N*-phenylhydroxylamine under visible light. *Green. Chem.* **23**, 3612–3622 (2021).
48. Xie, P. F. et al. Oxo dicopper anchored on carbon nitride for selective oxidation of methane. *Nat. Commun.* **13**, 1375 (2022).
49. Ghafari, H., Gorab, M. G. & Dogari, H. Tandem oxidative amidation of benzylic alcohols by copper(II) supported on metformin-graphitic carbon nitride nanosheets as an efficient catalyst. *Sci. Rep.-Uk.* **12**, 4221 (2022).
50. Vijeta, A., Casadevall, C. & Reisner, E. An integrated carbon nitride-nickel photocatalyst for the amination of aryl halides using sodium azide. *Angew. Chem. Int. Ed.* **61**, Advance Article <https://doi.org/10.1002/anie.202203176> (2022).
51. Mazzanti, S., Kurpil, B., Pieber, B., Antonietti, M. & Savateev, A. Dichloromethylation of enones by carbon nitride photocatalysis. *Nat. Commun.* **11**, 1387 (2020).
52. Wang, Y., Yao, J., Li, H., Su, D. & Antonietti, M. Highly selective hydrogenation of phenol and derivatives over a Pd@carbon nitride catalyst in aqueous media. *J. Am. Chem. Soc.* **133**, 2362–2365 (2011).
53. Elhage, A., Costa, P., Nasim, A., Lanterna, A. E. & Scaiano, J. C. Photochemical dehalogenation of aryl halides: importance of halogen bonding. *J. Phys. Chem. A.* **123**, 10224–10229 (2019).
54. McNesby, J. R. & Heller, C. A. Oxidation of liquid aldehydes by molecular oxygen. *Chem. Rev.* **54**, 325–346 (1954).
55. Jiang, H. Y. et al. Efficient photocatalytic chemoselective and stereoselective C–C bond formation over AuPd@N-rich carbon nitride. *Catal. Sci. Technol.* **11**, 219–229 (2021).
56. Dubey, A. V. & Kumar, A. V. A bio-inspired magnetically recoverable palladium nanocatalyst for the ullmann coupling reaction of aryl halides and arylboronic acids in aqueous media. *Appl. Organomet. Chem.* **34**, e5570 (2020).
57. Liu, Y. J., Zhang, D. M., Xiao, S. H., Qi, Y. & Liu, S. F. Copper-catalyzed homocoupling of alkyl halides in the presence of samarium. *Asian J. Org. Chem.* **8**, 858–862 (2019).
58. Lv, L. Y., Qiu, Z. H., Li, J. B., Liu, M. X. & Li, C. J. N₂H₄ as traceless mediator for homo- and cross- aryl coupling. *Nat. Commun.* **9**, 4739 (2018).
59. Han, F. Y., Xia, J. W., Zhang, X. L. & Fu, Y. S. PdAu alloy nanoparticles supported on nitrogen-doped carbon black as highly active catalysts for Ullmann coupling and nitrophenol hydrogenation reactions. *RSC Adv.* **9**, 17812–17823 (2019).
60. Lakshmi Devi, J. et al. WEPA: a bio-derived medium for added base, pi-acid and ligand free Ullmann coupling of aryl halides using Pd(OAc)₂. *Chem. Commun.* **54**, 12333–12336 (2018).
61. Xiao, G. et al. Visible-light-driven chemoselective hydrogenation of nitroarenes to anilines in water through graphitic carbon nitride metal-free photocatalysis. *Chem. Asian J.* **13**, 1950–1955 (2018).
62. Jia, Q. H. et al. Photocatalytic coupled redox cycle for two organic transformations over Pd/carbon nitride composites. *Catal. Sci. Technol.* **9**, 5077–5089 (2019).
63. Guo, Y. et al. Selectively catalytic hydrogenation of styrene-butadiene rubber over Pd/g-C₃N₄ catalyst. *Appl. Catal. A: Gen.* **589**, 117312 (2020).
64. He, H. Y. et al. Modulating the electrocatalytic performance of palladium with the electronic metal–support interaction: a case study on oxygen evolution reaction. *ACS Catal.* **8**, 6617–6626 (2018).
65. Liu, J. et al. Metal-free efficient photocatalyst for stable visible water splitting via a two-electron pathway. *Science* **347**, 970–974 (2015).
66. Liu, J. H., Zhang, Y. W., Lu, L. H., Wu, G. & Chen, W. Self-regenerated solar-driven photocatalytic water-splitting by urea derived graphitic carbon nitride with platinum nanoparticles. *Chem. Commun.* **48**, 8826–8828 (2012).
67. Chmiel, A. F., Williams, O. P., Chernowsky, C. P., Yeung, C. S. & Wickens, Z. K. Non-innocent radical ion intermediates in photo-redox catalysis: parallel reduction modes enable coupling of diverse aryl chlorides. *J. Am. Chem. Soc.* **143**, 10882–10889 (2021).
68. Suen, N. T. Electrocatalysis for the oxygen evolution reaction: recent development and future perspectives. *Chem. Soc. Rev.* **46**, 337–365 (2017).

Acknowledgements

The authors would like to thank the Key R & D and promotion projects in Henan Province (Grant No. 212102310372 (Y.R.)) and the Natural Science Foundation of Henan Province (Grant No. 212300410358(X.T.)).

Author contributions

Y.G. and X.T. performed the experiments. Y.-L.R. and X.T. wrote the paper. Y.-L.R., X.T., Y.G., W.A., Y.Q., X.Z., and C.N. conducted the data analysis. Y.-L.R. conceived the project. All authors discussed the results and commented on the paper.

Competing interests

The authors declare no competing interests.

Additional information

Supplementary information The online version contains supplementary material available at <https://doi.org/10.1038/s41467-022-33778-9>.

Correspondence and requests for materials should be addressed to Yun-Lai Ren.

Peer review information *Nature Communications* thanks the anonymous reviewers for their contribution to the peer review of this work.

Reprints and permission information is available at <http://www.nature.com/reprints>

Publisher's note Springer Nature remains neutral with regard to jurisdictional claims in published maps and institutional affiliations.

Open Access This article is licensed under a Creative Commons Attribution 4.0 International License, which permits use, sharing, adaptation, distribution and reproduction in any medium or format, as long as you give appropriate credit to the original author(s) and the source, provide a link to the Creative Commons license, and indicate if changes were made. The images or other third party material in this article are included in the article's Creative Commons license, unless indicated otherwise in a credit line to the material. If material is not included in the article's Creative Commons license and your intended use is not permitted by statutory regulation or exceeds the permitted use, you will need to obtain permission directly from the copyright holder. To view a copy of this license, visit <http://creativecommons.org/licenses/by/4.0/>.

© The Author(s) 2022